Proceedings of the ASME 2020
Verification and Validation Symposium
VVS2020
May 20-22, 2020, Virtual, Online

VVS2020-8812

RADIATION TRANSPORT SIMULATION RESULTS ASSESSMENT THROUGH COMPARISON WITH REDUCED COMPLEXITY ANALYTIC AND COMPUTATIONAL MODELS (LA-UR-20-22342)

Tyler J. Remedes *
Graduate Research Assistant,
Los Alamos National Laboratory
PhD Candidate,
University of Florida
tremedes@ufl.edu

Dr. Scott D. Ramsey
Los Alamos National Laboratory

Joseph H. Schmidt
Los Alamos National Laboratory

Dr. James Baciak
Professor, University of Florida

ABSTRACT

In the past when faced with solving a non-tractable problem, scientists would make tremendous efforts to simplify these problems while preserving fundamental physics. Solutions to the simplified models provided insight into the original problem. Today, however, the affordability of high-performance computing has inverted the process for analyzing complex problems. In this paradigm, results from detailed computational scenarios can be better assessed by "building down" the complex model through simple models rooted in the fundamental or essential phenomenology.

This work demonstrates how the analysis of the neutron flux spatial distribution behavior within a simulated Holtec International HI-STORM 100 spent fuel cask is enhanced through reduced complexity analytic and computational modeling. This process involves identifying features in the neutron flux spatial distribution and determining the cause of each using reduced complexity computational and/or analytic model. Ultimately, confidence in the accuracy of the original simulation result is gained through this analysis process.

1 Introduction

There is inherent confidence in the results of simulation when using a tool such as Monte Carlo N-Particle (MCNP) radiation transport program, which has been extensively verified and validated [1]. However, users of computational codes are always trying to simulate new, more complex, or more detailed problems, thus adding stress on both the code and computational resources. When these resources are limited, a user will have to make concessions by simplifying the problem while trying to preserve details important to the specific question. In the context of MCNP, simplifications typically come as reductions in geometry, or by using variance reduction techniques. Both approaches enable a user to unknowingly influence the physics of the problem, leading to potentially inaccurate or non-physical results. Errors can also be introduced as a result of faulty input into a computational tool: something as simple as transposing numbers in a tally input could result in incorrect answers. Methods used by previous generations of scientists provide a foundational approach to address these issues and simultaneously gain confidence in both computational and analytic modeling.

In the past, when faced with non-tractable problems, scientists would make tremendous efforts to simplify them and generate simpler models that preserved the fundamental physics. This process involved applying assumptions and simplifications

*Address all correspondence to this author.

to slowly reduce the complexity of the problem until it reached a solvable form. Each assumption and simplification was chosen and applied with the intent to preserve the essential physics of the problem, since, if the core physics of the problem were eliminated, the simplified model served no purpose. Moreover, if done correctly, solutions to the reduced model would serve as useful approximations of the original problems. In a sense, solving the simple models laid the ground-work for and provided insight into the more complex problem. Today, however, the affordability of high performance computing has essentially replaced the process for analyzing complex problems. Rather than "building up" a problem by understanding smaller, simpler models, a user generally relies on powerful computational tools to directly arrive at solutions to complex problems.

In this paradigm, reduced complexity computational and analytical models still have an important purpose. The explicit form of an analytic solution is arguably the best way to understand the qualitative properties of simple models [2]. In contrast to "building up" a complex problem through understanding simpler problems, results from detailed computational scenarios can be better explained by "building down" the complex model through simple models rooted in the fundamental or essential phenomenology. Simplified analytic and computational models can be used to 1) verify computational tools [3], 2) increase a user's confidence in the computational solution of a complex model, 3) confirm there are no user input errors, and 4) ensure the physical assumptions essential to the simulation tool were preserved. The final three items in the previous list will be the focus of this work.

The "simulation results assessment methodology", or simply "results assessment methodology", presented in this work acts complimentary to existing techniques - verification, validation, and uncertainty quantification - to add additional robustness to the analysis of simulation results. The purpose of this work is to increase confidence that a simulation will produce reliable results through qualitative and semi-quantitative analyses as demonstrated through the rigorous analysis of the neutron flux behavior within the fuel region of a Holtec International HI-STORM 100 used fuel cask.

As an example of the utility of the results assessment methodology, this work evaluates the simulated neutron flux spatial distribution interior to a Holtec HI-STORM 100 spent fuel cask using the previously discussed framework. Features of the interior neutron flux spatial distribution are identified from the results of a detailed MCNP simulation. These features are locations in the neutron flux spatial distribution that have some identifiable shape against which results from simplified models can be compared. Four features are identified and analyzed using a combination of simplified analytic and computational models. The analysis is enhanced through complementary, reduced complexity analytical, computational modeling and confidence in gained in the accuracy of the original simulation.

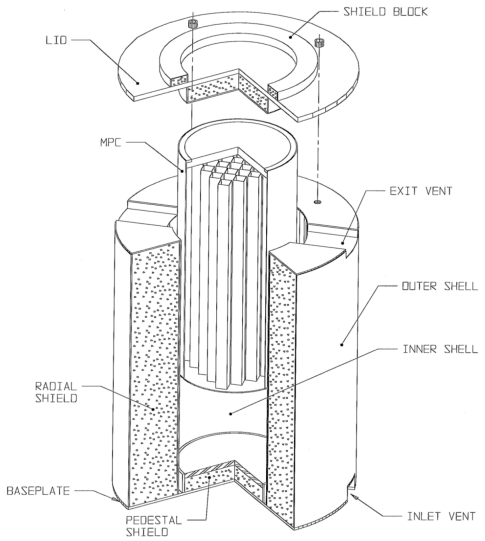

FIGURE 1: The Holtec HI-STORM 100 spent fuel cask system is designed to protect fuel, transfer decay heat to the environment, prevent proliferation of nuclear material, and attenuate radiation [4]. The multipurpose cask is seen partially inserted into the steel and concrete overpack. Current designs of the HI-STORM 100 do not use the inner shell and therefore, the inner shield is not modeled in MCNP.

1.1 Description of HI-STORM 100

Dry storage casks are used to store nuclear fuel rods which have been irradiated in a power reactor and have been cooled in a fuel storage pond. The fuel is highly radioactive after being removed from a reactor. Storing used nuclear fuel has become a challenge in the United States since there is no long-term storage location for it. Instead, spent nuclear fuel is stored in dry storage casks at the facility where it was generated. These casks are designed to overcome the challenges involved in storing spent nuclear fuel: shielding radiation, conducting decay heat away from fuel rods, protecting spent nuclear fuel from damage, and preventing proliferation of nuclear materials. This work is only concerned with the radiation shielding capabilities of a spent fuel cask.

Figure 1 is a diagram of the Holtec International HI-STORM 100 spent fuel canister system. The HI-STORM 100 canister system is the most used spent fuel storage system in the United States with 750 canisters having been loaded before 2017 [5]. The fuel is stored in the multi-purpose canister (MPC) which is shown partially inserted in Fig. 1. The MPC houses spent fuel in a honeycomb fuel basket (Fig. 2) with each cell containing a

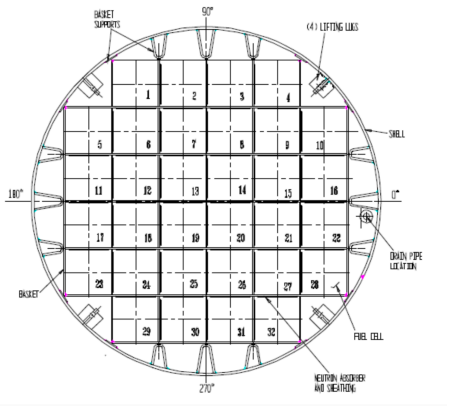

FIGURE 2: A cross section view of the multi-purpose canister. While there are multiple designs which accommodate different amounts of fuel, the MPC-32 is chosen for this work [4]. The MPC-32 is capable of holding 32 fuel bundles, one bundle in each square lattice element. The fuel basket and cylindrical wall of the MPC are made using stainless steel 304 and the canister is sealed by welding a baseplate to the bottom and a lid and closure ring to the top of the cylinder respectively.

single fuel bundle. The MPC is surrounded by the HI-STORM overpack. The overpack consists of two parts: a cylindrical dual material structure welded to a baseplate and a dual material removable lid. Both parts of the overpack use a combination of concrete and carbon steel to shield radiation, protect the MPC, and prevent proliferation of nuclear material. Four vents are located at both the top and bottom of the overpack which allow air to circulate between the overpack and MPC, removing heat caused by decaying isotopes in the spent fuel.

As attending plant workers must be protected from the radiation field produced by spent nuclear fuel rods, opening a sealed MPC is an expensive and potentially dangerous task. Therefore, alternative methods are being explored to ensure the content and integrity of fuel components without opening a cask. A sample of these techniques includes fast neutron spectroscopy using an exterior source [6], deduction of interior structure based on exterior dose rates [7], and neutron based computer tomography [8]. Each of these techniques simulates nondestructive evaluation using various radiation source definitions, virtual detectors, and simulated cask designs to determine specific quantities related to the neutron flux within the spent fuel cask. Therefore, the key metric of this work is the interior neutron flux spatial distribution of the HI-STORM 100 spent fuel cask, as this quantity is shared among research in spent fuel casks. Simulation tools have become an important part of investigating the efficacy of a nondestructive evaluation technique, and ensuring the accuracy of these results is even more important since experimental data associated with the techniques is limited.

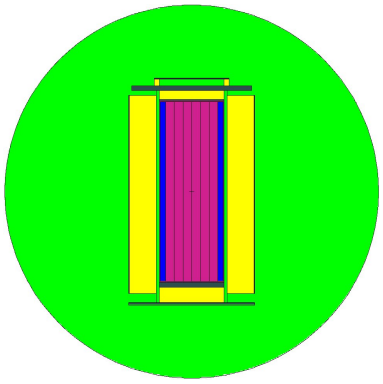

FIGURE 3: The side view of the HI-STORM 100 spent fuel cask (MPC and overpack) modeled in MCNP. This is the detailed model.

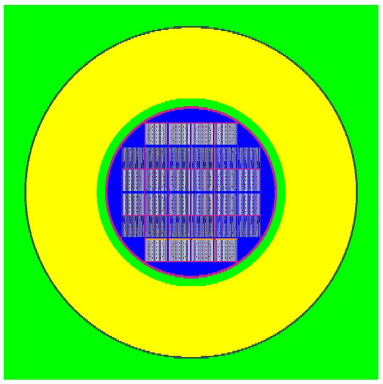

FIGURE 4: The top view of the HI-STORM 100 spent fuel cask modeled in MCNP. This view shows the fuel arrangement of the detailed model.

The MPC and overpack are modeled in the Monte Carlo N-Particle (MCNP) program to determine the simulated interior neutron flux spatial distribution averaged over the height of the cask as a function of radial distance from the centerline [1]. Figures 3 and 4 show, respectively, a side view and cross section of the cask geometry simulated in MCNP. This model is called the "detailed model" throughout this work and models the geometry of the cask down to the individual fuel rod level. Each fuel rod acts as a source term for neutrons produced from spontaneous fission and (α, n) reactions.

Figure 5 shows a single fuel cell cross section from the detailed model. The fuel cell contains two neutron absorbing pads composed of boron-carbide and aluminum, 264 fuel rods with zircalloy cladding and 25 water rods representing instrumentation. Fuel rod composition is determined using data from the Next Generation Safeguards Initiative which analyzed the composition of Westinghouse 17x17 fuel bundles with various de-

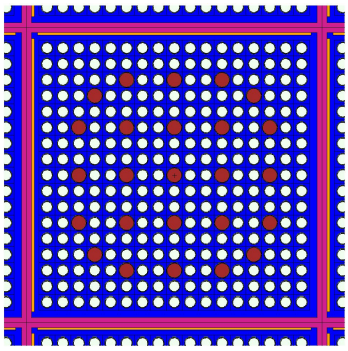

FIGURE 5: The zoomed in image of a single fuel cell cross section in the detailed model. There are neutron absorbing pads (orange rectangles) placed along the interior left and upper faces of the fuel basket (pink rectangles). Fuel rods (small circles) include a fuel region, helium gap, and cladding. The larger circles are the cross sectional view of water cylinders which represent instruments used for monitoring the safety of the HI-STORM 100 spent fuel cask system.

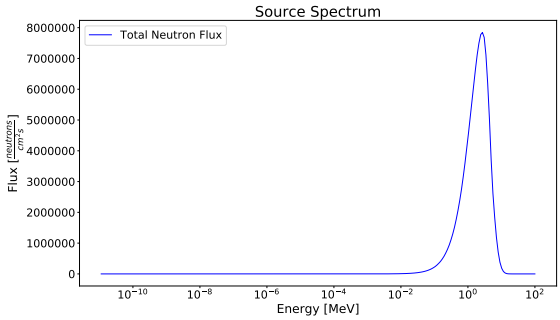

FIGURE 6: The source spectrum used in MCNP simulations. The spectrum is a result of spontaneous fission and (α, n) reactions.

grees of initial ^{235}U enrichment and burn-up values. This work investigates fuel with an initial enrichment of 3% ^{235}U and a burn-up value of 30 GWd/MTU [9]. The composition of each individual fuel rod is unique, since fission fragments distribution is probabilistic, which introduces variance in the local neutron flux. An average fuel rod composition is determined based on the weight of each isotope present in a single spent fuel bundle. This average fuel rod composition is used for all fuel rods in the simulation in order to investigate the effects of geometry, detail, and non-fuel materials without influence from loading patterns of specific fuel rods.

Given the presence of various fission product isotopes in the fuel rods, the associated intrinsic neutron source is included via an MCNP neutron source definition. This definition is found using the ORIGEN-S 0-dimensional irradiation and decay code supplied with the SCALE package from Oak Ridge National Laboratory [10]. The neutron energy spectrum associated with the intrinsic source is shown in Fig. 6. The source spectrum results from spontaneous fission of isotopes in the fuel (such as ^{252}Cf) and (α,n) reactions occurring in the irradiated fuel.

As calculated using MCNP, Fig. 7 depicts the height-averaged scalar neutron flux as a function of radial position within the HI-STORM 100 spent fuel cask. The color of the line is related to the material through which the neutron flux is being simulated: fuel is green (the entire area interior to the MPC is considered the fuel region), MPC is blue, air is grey, concrete is red, and carbon steel is black. The vertical lines designate interfaces between material boundaries. Figure 7 shows about half of the neutron flux is attenuated in the fuel region, and the concrete further reduces the flux by two orders of magnitude. This result is intuitively sensible: the fuel region is comparatively dense and composed of neutron-absorbing materials (e.g., boron), while the thick concrete overpack region is composed principally of highly thermalizing isotopes (e.g., hydrogen). Together, these processes are indicative of the observed dramatic reduction in neutron flux throughout the cask. The dense fuel with a propensity to absorb neutrons and the highly scattering concrete account for nearly all the reduction in neutron flux. However, advancing beyond intuition requires definitive answers to a variety of additional questions, namely:

1. Are the results correct?
2. Could a mistake have been made in the simulation input?
3. Was an assumption made that neglected important physics?
4. Does the problem include physics or exist in a physical regime outside the viability of the simulated tool used?

While corroborating a simulation result with intuition is qualitatively valuable, quantitative assessments and their associated effects on confidence in simulation results demands that the preceding questions be comprehensively addressed. The purpose of this work is to answer these questions by 1) identifying key features of the neutron flux spatial distribution as simulated in the detailed model, 2) developing simple physical models to determine the cause of each feature, and 3) gain confidence in the accuracy of the solution and inerrancy of the simulation process.

2 Identification of Features

"Features" are locations in the simulated neutron flux spatial distribution shown in Fig. 7 which appear to be the result of a physical process. Using a reduced complexity analytic or computational model to reproduce a feature yields two benefits: 1) the physical process that generates the feature in question is identified and, 2) confidence is gained in the accuracy of the simula-

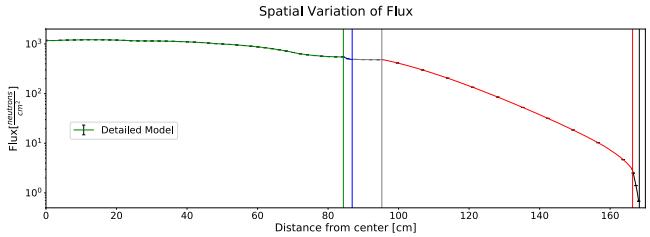

FIGURE 7: The interior neutron flux spatial distribution of the simulated HI-STORM 100 spent fuel cask. The vertical lines represent interfaces between material regions.

tion result. Confidence in the simulation result is gained because a feature is determined to be a result of an understood physical process. That is, the feature should exist in the problem, is being modeled correctly in the code, and is not a computational artifact. Ensuring agreement between simplified and complex models also corroborates the accuracy of the simulation input itself. Something as simple as inputing an incorrect area or volume would not result in a fatal error message in MCNP, but would lead to incorrect neutron flux results. The process of reproducing features using simplified analytic and computational models provides an opportunity to identify errors in the simulation input and addressing these errors leads to increased confidence in the accuracy of a simulation.

There are four features discussed in this paper which are identified as:

1. The "flat" flux region (highlighted in Fig. 8): The flux in this region smoothly decreases by approximately 36% even though intuition suggests the flux should increase in the fuel pins and decrease in the space between fuel pins.
2. The abrupt level-off region (highlighted in Fig. 9): The flux only decreases $\sim$3 % over the region 65 cm $\leq r \leq$ 84.1 cm from the cask centerline.
3. Periodic depressions (highlighted in Fig. 10): There is a $\sim$2% reduction in the flux near 25 cm, 50 cm, and 75 cm from the cask centerline.
4. The asymmetric flux: Figure 11a is a density plot of the neutron flux when looking at a center slice of the cask from above. Figure 11b is a contour plot to better illustrate the neutron flux asymmetry present in Fig. 11a. The neutron flux in the upper left section (above the diagonal line) of the plot is less than the neutron flux in the lower right section (below the diagonal line) of the image. The asymmetry occurs throughout the entire fuel region but is most obvious in the region exterior to the fuel lattice - the dark blue vs. light blue regions in Fig. 11a and the black vs. white regions in Fig. 11b.

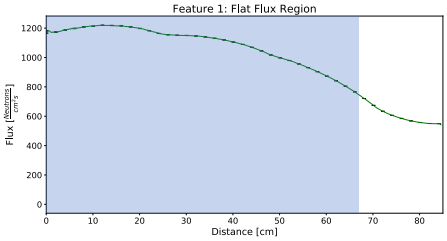

FIGURE 8: The neutron flux spatial distribution between the cask centerline and inner face of the MPC. The highlighted region is considered the flat flux region. This neutron flux is relatively flat and does not vary on the same order as the physical dimensions of materials in this region.

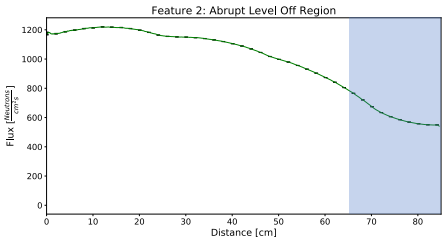

FIGURE 9: The flux stops decreasing and instead levels-off in the abrupt level-off region. The flux decreases less than 3% over the last ten centimeters before the interface between the fuel region and MPC.

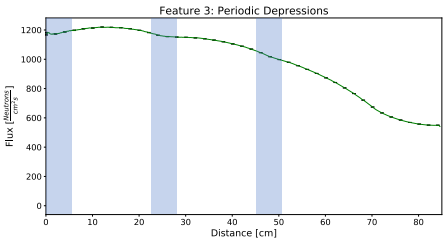

FIGURE 10: There are three depressions in the neutron flux spatial distribution located approximately 22 cm apart. The flux decreases about 2% at each depression.

3 Results and Discussion

Initially, the flatness of the first feature suggests that a reduction in fine structure detail can be used to adequately represent a substantial portion the fuel region. Each fuel pin is approximately 1cm in diameter, yet the neutron flux spatial distribution does not show variations at the centimeter level. Fluctuations in the neutron flux spatial distribution at the centimeter level would require any simplified models to also preserve geometric struc-

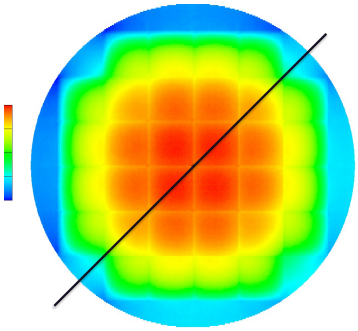

(a)

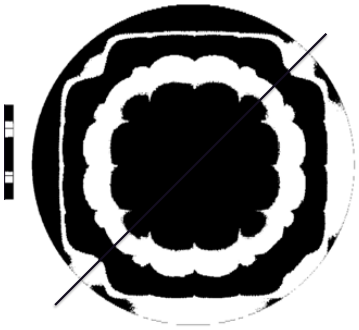

(b)

FIGURE 11: (a) A density plot of the neutron flux at a "central slice" of the fuel cask as viewed from above. This plot shows the neutron flux is less in the upper left section than in the lower right section. The asymmetry is most evident in the blue and light blue sections at the outer radius of the figure. (b) A contrast plot emphasizing the asymmetry of the flux values.

tures at the centimeter level, but the absence of these fluctuations implies that geometric reductions are possible. The total mean free path (mfp) - or average distance a neutron travels between interactions - is used to identify where these fine structure reductions can credibly be made. Figure 12 shows the mfp of neutrons as a function of neutron energy in both the fuel rods and in helium. At all neutron energy values, the mfp for a neutron of any energy is approximately 50,000 times greater in helium than in the fuel rods. Since the mfp of neutrons is much greater than the distance between fuel rods, the probability of neutron interactions occurring in the helium is assumed to be negligible. Consequently, a reduced-complexity computational model includes a fuel region filled with a single homogeneous fuel material, where the density and composition of this new homogeneous fuel is changed to account for all materials in the fuel region.

For the purpose of clarity, this fuel composition is called "fully homogenized" since it incorporates all the materials inside

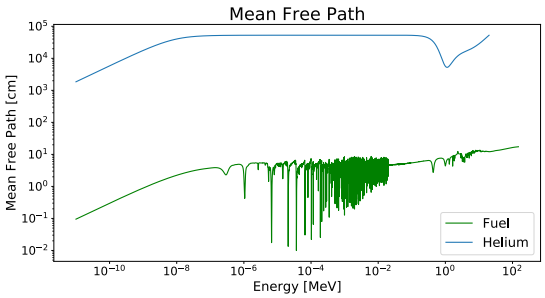

FIGURE 12: The mean free path of neutrons in helium (blue) is more than 50,000 times greater than in a fuel pin (green).

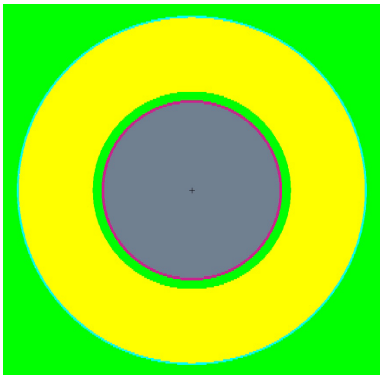

FIGURE 13: The homogeneous model. The gray circle is the fully homogenized fuel which fills the entire volume interior to the MPC.

the MPC. The fully homogenized fuel composition is determined by calculating the mass fractions of each material in the MPC (the stainless steel basket, the neutron absorbing pads, the helium backfill, and the fuel rods). Finally, the density of the fully homogenized fuel is corrected to account for the various densities of each material in the MPC (10.44 $\frac{g}{cm^3}$ for a single fuel rod vs. 2.31 $\frac{g}{cm^3}$ for the fully homogenized fuel). The entire interior volume of the MPC is filled with the fully homogenized fuel material. Figure 13 is a cross section view of the corresponding MCNP model using the fully homogenized fuel material. This model is referred to as the "homogenous model".

Figure 14 shows the homogeneous model neutron flux spatial distribution through the fuel region of the MPC, together with the complementary result from the detailed model. The homogeneous model overpredicts the neutron flux spatial distribution through the fuel region by 20-25% (where percent differences are defined as the ratio of the difference between the fluxes from the simplified and detailed models). Even though the reduced model overpredicts the detailed flux, the shape of the neutron flux spatial distribution predicted in both models shows a steady decrease across the inner 65 cm. The relative flatness of the two

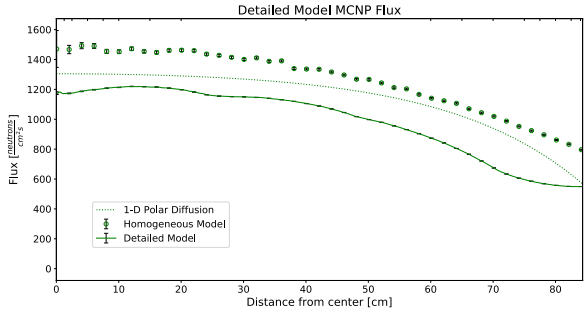

FIGURE 14: The results of the simulated neutron flux spatial distribution from the homogenous model (circles) is similarly flat to the neutron flux spatial distribution of the detailed model (solid line). The flux calculated using the diffusion approximation (dotted line) is also plotted against the two MCNP models. The diffusion approximation also shows the flatness of the neutron flux spatial distribution.

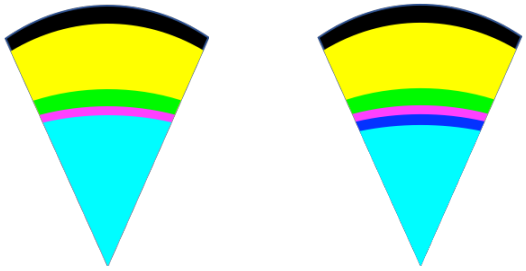

FIGURE 15: Section views of the (a) homogeneous model and (b) helium model. The helium model includes an annulus of helium gas, ∼10 cm thick, added around the homogenized fuel to allow streaming at the edge of the fuel region. Not to scale.

fluxes is evidence that geometric attenuation is less important than the material properties within the MPC. To further corroborate this notion, Fig. 14 also includes results from an analytic model: the dotted line appearing in this figure is a result from monoenergetic, 1D cylindrical diffusion theory [11]. In this analytic setting, the monoenergetic scalar neutron flux across a 1D cylindrical region with constant material properties is given by

$$\phi(r) = \frac{S}{DB^2}\left(1 - \frac{I_0(Br)}{I_0(B\tilde{r})}\right); \qquad B \equiv \sqrt{\frac{\Sigma_a - \bar{\nu}\Sigma_f}{D}}. \qquad (1)$$

where S is the intrinsic neutron source, B is the material buckling as indicated in terms of the macroscopic total absorption cross section Σ_a, macroscopic fission cross section Σ_f, and mean number of neutrons per fission $\bar{\nu}$, and diffusion coefficient D, I_0 is the modified Bessel function of the first kind, and $\tilde{r}$ is the extrapolated radius of the fuel region. The spatial curvature of the scalar flux appearing in Eq. 1 is controlled principally by the material buckling B; as the value of B increases (resulting when absorption physics is dominant over scattering physics) the neutron flux spatial distribution calculated in Eq. 1 produces a flat distribution in r - as in fuel region of both computational models. The flatness of the diffusion model is proof that the flatness seen in the MCNP models is due to material properties being dominant over geometry. While the diffusion model captures the essential physics giving rise to the flat flux region, it does not adequately capture the abrupt level off within the fuel region for $r > 65$cm.

In order to better capture the physics which describes the second feature, a second model is developed. The purpose of this model is to capture the physics associated with the neutron flux spatial distribution suddenly flattening before exiting the MPC. Intuitively, since geometric attenuation is minimal and the mfp for neutrons (∼70,000 cm at 1 MeV) is much greater than the thickness of the region between the fuel basket and MPC wall (∼0 cm), a free streaming (i.e., constant flux) approximation is likely to be valid there. To corroborate this notion, the homogeneous model is further modified to add an annulus of helium around a fuel region which is reduced in radius in a manner which preserves the volume of the original 32 fuel cells. This model is referred to as the "helium model" (Fig. 15). The composition of the fuel region is changed to account for the helium now present in the annulus. The new homogenized fuel composition, called the partially homogenized fuel composition, is made using the mass fractions of materials in the 32 fuel cells (the stainless steel fuel basket, the neutron absorbing pads, the helium interior to the fuel cells, the fuel rods) and the density of the material is adjusted to account for the reduced amount of helium (2.95 $\frac{g}{cm^3}$).

Figure 16 shows the results of the simulated flux in the helium model as compared to the detailed model. The fuel region, comprised of partially homogenized fuel material, has a smaller radius and the analytic solution is held constant for $r > \tilde{r}$. The increased density of the fuel in the helium model increases the total neutron absorption and thus lowers the amplitude of the neutron flux spatial distribution. The flux flattens out over the last 20 cm, which is a result of adding the non-interacting helium annulus. The helium model better demonstrates that the flatness of the two MCNP models and the analytic model match, with the exception of the three depressions present in the detailed models. These results do show neutrons streaming through the helium region exterior to the fuel cells before exiting into the MPC even though the helium model and the analytic model do not capture the small depressions.

To this point, the simulation results assessment has shown that explanation of causes for the first two features does not necessitate simulation of geometric details at the individual fuel pin level. However, the physics associated with the three small de-

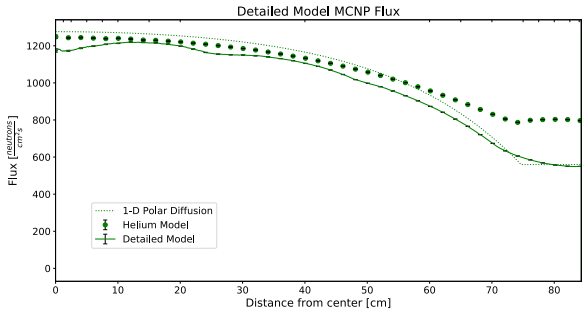

FIGURE 16: The neutron flux spatial distribution simulated by the helium model (circles) captures the neutron flux spatial distribution flattening out in the detailed model (solid line) over the 20 cm region before exiting the fuel region. The diffusion approximation (dotted line) also captures the flux flattening near 65 cm from the cask centerline after adding a helium annulus for neutron streaming.

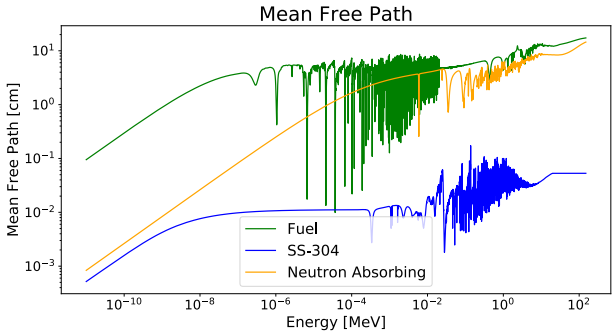

FIGURE 17: The mean free paths for stainless steel 304 (blue), neutron absorbing pad material (orange), and fuel pin material (green). These three mean free paths are similar to the physical thicknesses of each material implying that the steel and neutron absorbing pads need to be included in MCNP simulations as discrete materials instead of being incorporated into the homogenized fuel.

pressions in the detailed model (seen in Fig. 10) has not been explained. Intuition suggests it seems necessary that some level of geometric detail needs to be added back into the reduced complexity simulations to identify the cause of the final two features.

The scalar flux depressions depicted in Fig. 10 represent the third feature and are presumed to be caused by the neutron absorbing pads that are present between fuel bundles, located at $-71.62 < x < -71.41$ cm, $-47.61 < x < -47.40$ cm, $-23.61 < x < -23.40$ cm, $0.40 < x < 0.61$ cm, $24.40 < x < 24.61$ cm, $48.41 < x < 48.62$ cm. These pads contain ^{10}B, which is a highly neutron absorbing material. To corroborate this notion, reintegrating the stainless steel basket structure and neutron absorbing pads is expected to capture the depressions not found in the previous models. Again, comparing the mfp of neutrons in stainless steel 304, the neutron absorbing pads, and fuel rods in Fig. 17 shows the mfp is dominated by the absorbing component at a level of approximately 10 cm (or less, depending on the energy of the incident neutrons). These mfp's are similar to the physical thickness of the stainless steel, neutron absorbing pads, and fuel in the MPC. Therefore, the neutrons will undergo an appreciable number of interactions in the stainless steel and neutron absorbing materials. However, unlike in the fuel, no neutrons are being generated in the steel and neutron absorbing materials, and so the flux is expected to decrease therein.

Another MCNP model is developed to describe the cause of the depressions, Fig. 18. This multi-layered model is called the "1-D basket model" and represents a single row of fuel cells from the detailed model with one difference: the volume attributed to fuel materials. In this model, the interior volume of each fuel cell contains a cell homogenized fuel composition with helium on both sides and neutron absorbing pad to the left. The cell homogenized fuel composition is determined using the mass fraction of materials which comprise the 264 fuel rods and helium between the fuel rods in each cell. The volume of the cell homogenized fuel material is defined to be equal to the volume of a single fuel bundle.

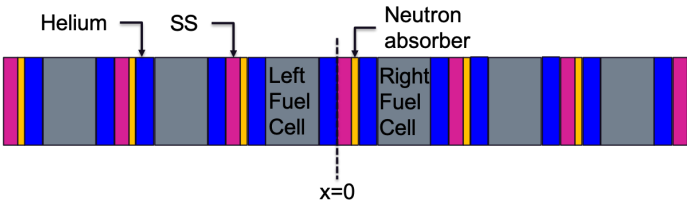

FIGURE 18: The 1-D basket model used to identify the cause of the small depressions. The model is repeating layers of stainless steel (pink), neutron absorbing pads (orange), helium (blue), and cell homogenized fuel (gray).

The simulated neutron flux spatial distribution through the 1-D basket model is shown in Fig. 19. The simplified basket model has six small depressions present in the flux around ± 25 cm, ± 50 cm, ± 75 cm. These depressions correspond to a 1-2% local reduction in the flux, which is similar in location and magnitude to the depressions present in the simulated neutron flux spatial distribution in the detailed model. The depressions in the neutron flux spatial distribution occur within the stainless steel and neutron absorbing pad materials. The flux increases in the fuel as neutrons are born from spontaneous fission decays and (α, n) reactions. The combination of the absorption events in the neutron absorbing pads and source events in the fuel cause the depressions observed in the neutron flux spatial distribution.

The final feature, the flux asymmetry (seen in Fig. 11), is

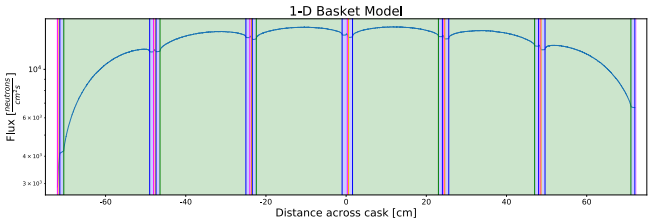

FIGURE 19: The neutron flux spatial distribution simulated from the 1-D basket model. The colors are representative of each material: stainless steel 304 (pink), neutron absorbing pad (orange), helium (blue), and cell homogenized fuel (green). There are depressions present in the flux which occur within the stainless steel and neutron absorbing pads.

also explained using the 1-D basket model. The detailed model shows a higher flux leaving the bottom right section of the cask as compared to the top left section of the cask. Fig. 19 shows the same behavior. The leftmost face has a lower exiting flux value than the value observed at the rightmost face. Figure 18 also shows the reason for the asymmetry: a neutron born in the left fuel cell and traveling left will pass through three neutron absorbing pads before exiting the left face, which is the same number of neutron absorbing pads that same neutron would have to pass through if it were traveling right. Conversely, if a neutron is born in the right fuel cell and traveling to the left, it passes through four neutron absorbing pads. However, if that same neutron were to travel right, it only potentially encounters two neutron absorbing pads. The number of neutron absorbing pads a neutron potentially encounters is not the same based on the the location of neutron generation and direction of travel because of the placement of neutron absorbing pads in the MPC. The asymmetric loading of these pads directly affects the neutron flux spatial distribution exiting the spent fuel cask.

To further corroborate this notion, the detailed model was adjusted, replacing the stainless steel structure and neutron absorbing pads with vacuum. Figure 20 compares the ratio of the neutron flux spatial distribution averaged over the top left section and the flux averaged over the bottom right section from the detailed model where one simulation replaced neutron absorbing pads with vacuum and the original detailed model. The maximum deviation of the ratios of neutron flux spatial densities is 0.1% as a result of replacing non-fuel structure in the MPC with vacuum, confirming the results from the basket model. In contrast, the maximum deviation of these same ratios in the original detailed model is nearly 10%.

Previous findings have shown that geometric structures finer than the stainless steel baskets, neutron absorbing pads, and helium annulus are unnecessary for characterization of the spatial flux distribution arising from the detailed model. A final model, the "cruciform model", is developed to ensure no important physics are neglected in the reduced-order modeling and analysis process. This model uses the cell homogenized fuel definition in each of the 32 original fuel cells. In doing so, the stainless steel fuel basket and neutron absorbing pads are retained and discrete from the homogenized fuel. The helium surrounding the 32 fuel cells is also retained.

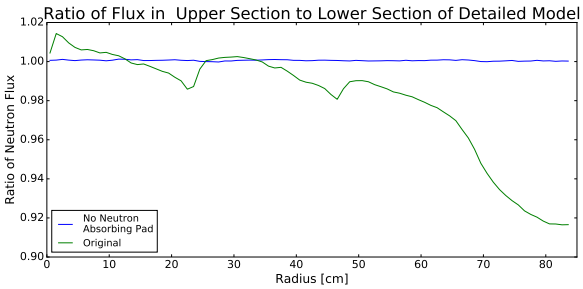

FIGURE 20: The ratio of the neutron flux spatial distribution in the upper left section of the fuel region to the neutron flux spatial distribution in the lower right section of the fuel region. This ratio is nearly 1 over the entirety of the fuel region, confirming the assumption that removing the neutron absorbing pads removes the previously identified depressions.

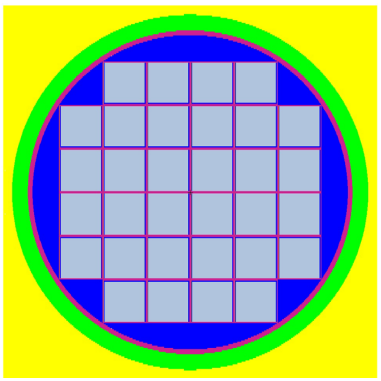

FIGURE 21: The cruciform model. The gray squares are cell homogenized fuel, the stainless steel fuel basket and MPC are pink, the helium annulus is blue, the air exterior to the MPC is green, and concrete is yellow. The neutron absorbing pads (orange) are present in this diagram, but are too thin to be seen here.

Figure 22 shows the neutron spatial flux distribution simulated by the cruciform model underpredicts the flux from the detailed model by 5-7% through the entire fuel region. Moreover, these results can also be interpreted as the cruciform model accounting for the physics relevant to the detailed model's spatial neutron flux distribution at a level greater than 90%. Any further additions of fine details will "close the gap" between the detailed and cruciform models at a sub-10% level.

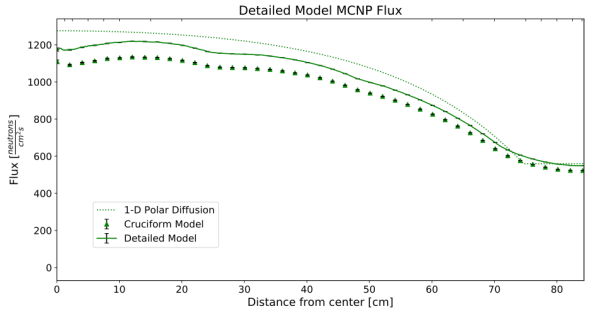

FIGURE 22: The neutron flux spatial distribution of the cruciform model (triangles) capture the flatness of, the leveling off of, and the depressions in the neutron flux spatial distribution seen in the detailed model (solid).

4 Conclusions

Using reduced complexity analytic and computational models to analyze the simulation results of a high-fidelity computational model allows for the quantification of effects of any assumptions invoked when developing the latter model. Ensuring important physics are preserved in the course of conducting simulations increases the likelihood of correct results. This work exemplified this notion through a process referred to as "simulation results assessment." As a demonstration, this work included post-simulation analysis of a detailed MCNP model of a HI STORM 100 spent nuclear fuel cask. A series of reduced analytic and computational models were developed and used to identify the physics which causes features in the neutron flux spatial distribution as calculated by the detailed model. In the HI-STORM 100 model, the stainless steel basket, neutron absorbing pads, and helium annulus around the fuel cells are important physical components that need to be preserved in modeling. Retaining the individual fuel pin structure was found to be less important than broadly capturing the lumped material properties inside the individual fuel cells. These results were corroborated using the cruciform model, which appears to capture the physics relevant to the neutron flux spatial distribution in the detailed model beyond the 90% level. The major features of the neutron flux spatial distribution simulated by the detailed model are expected to be correct since the this model preserves material fuel properties and the geometric structure of the neutron absorbing pads and helium annulus.

4.1 Future work

Future work continues the current analysis through the overpack region of the spent fuel cask. To further enhance the analysis, analytic and reduced computational models will be used in a rigorous quantitative sensitivity analysis study to identify the parameters to which the system is most sensitive. The accuracy of simulation results are further ensured by identifying the most sensitive parameters in the detailed model and reduced analytic and computational models and ensuring no approximations affect those sensitive parameters. The results assessment methodology and proposed sensitivity analysis study will act complimentary to existing verification, validation, and uncertainty quantification techniques by further elucidate post-simulation analysis activities.

ACKNOWLEDGMENT

This work was supported by the US Department of Energy through the Los Alamos National Laboratory. Los Alamos National Laboratory is operated by Triad National Security, LLC, for the National Nuclear Security Administration of the U.S. Department of Energy (Contract No. 89233218CNA000001).

REFERENCES

[1] Werner, C., and et. al., 2018. Mcnp6.2 release notes. report LA-UR-18-20808, Los Alamos National Laboratory.

[2] Barenblatt, G., 2014. *Flow, Deformation, and Fracture: Lectures on Fluid Mechanics and the Mechanics of Deformable Solids for Mathematicians and Physicists*. Cambridge University Press.

[3] Grechanuk, P., and et al., 2017. "Semi-analytic benchmarks for mcnp6". *2017 American Nuc. Soc. Annual Meeting*(LA-UR-17-20668).

[4] , 2017. Hi-storm fsar. report, Holtec International.

[5] JR., R. H. J., 2016. Dry cask inventory assessment. Tech. rep., Savanah River National Laboratory.

[6] Harkness, I., and et. al., 2018. Feasibility of fast neutron spectroscopy for safegaurds and verification of spent fuel in dry cask storage. Tech. Rep. LA-UR-18-29519, Los Alamos National Laboratory.

[7] Gao, Y., and et. al., 2018. "Radiation dose rate distributions of spent fuel casks estimated with mavric based on detailed geometry and continuous-energy". *An. of Nuc. Eng.*(117), pp. 84–97.

[8] Greulich, C., and et. al., 2017. "High energy neutrons transmission analysis of dry cask storage". *Nuc. Inst. and Meth. in Phys. Res. A,* **874**, pp. 5–11.

[9] Trellue, H. R., and et. al., 2011. Description of the spent nuclear fuel used in the next generation safegaurds initiative to determine plutonium mass in spent fuel. report, Los Alamos National Laboratory.

[10] , 2011. Scale: Comprehensive modeling and simulation suite for nuclear safety analysis and design. report, Oak Ridge National Laboratory.

[11] Lamarsh, J. R., and Baratta, A. J., 2001. *Introduction to Nuclear Engineering*. Prentice Hall.